Convex Optimization of Coincidence Time Resolution for High Resolution PET Systems

Paul D. Reynolds, *Student Member, IEEE*, Peter D. Olcott, *Student Member, IEEE*, Guillem Pratx, *Student Member, IEEE*, Frances W.Y. Lau, *Student Member, IEEE* and Craig S. Levin, *Member, IEEE*

***Abstract*–We are developing a dual panel breast-dedicated PET system using NOVA RENA-3 ASICs. The coincidence timing resolution of the RENA-3 ASIC can be improved with list mode calibration. We treat the calibration problem as a convex optimization problem and use the RENA-3's analog based timing system to correct the measured data for time dispersion effects from correlated noise, position sensitive avalanche photodiode (PSAPD) signal delays and varying signal amplitudes. The direct solution to the optimization problem involves a matrix inversion that grows order (n^2) with the number of parameters. An iterative method using single-coordinate descent to approximate the inversion grows only order (n). The system calibration method is demonstrated with measured pulser data as well as with two LSO-PSAPD detectors in electronic coincidence. After applying the algorithm, the 511keV photopeak paired coincidence time resolution from the LSO-PSAPD detectors under study improved by 57%, from raw value of 16.3±0.07 ns FWHM to 6.92±0.02 ns FWHM (11.52±0.05 ns to 4.89±0.02 ns for unpaired photons).**

I. Introduction

We are developing Positron Emission Tomography (PET) systems for small animal imaging and for breast cancer imaging. The latter system comprises a two-panel geometry. Each of the two 16cm x 9cm x 2cm detector panels require 2304 Position Sensitive Avalanche Photodiodes (PSAPDs) coupled to 8x8 1x1x1 mm^3 LSO (Lutetium Oxyorthosilicate) scintillation crystal arrays for a total of 294912 crystals. The system uses the 36 channel RENA-3 readout ASIC, developed by NOVA R&D, for readout and acquires list-mode data.

PET systems are typically calibrated for time delay offsets for each detector prior to scans. Originally, individual detector blocks were calibrated using manual methods or later, using algorithms and timing histograms to calibrate offsets for each block detector [1],[2],[3], and then for each individual crystal [4].

We show that per crystal coincidence time calibration is a convex optimization problem, which can be formulated using data from a list-mode acquisition, and solved with a direct solution, as well as with standard convex optimization techniques. We also demonstrate that additional correlated noise can be accounted for to further improve the annihilation photon pair coincidence time resolution.

Manuscript received November 4, 2008. This work was supported in part by NIH Grants R01 CA119056, R33 EB003283, R01 CA120474.

P. D. Reynolds is with the Department of Electrical Engineering, Stanford University, Stanford, CA 94305 USA (e-mail: paulr2 @stanford.edu).

P. D. Olcott is with the Bio-Engineering Department, Stanford University, Stanford, CA 94305 USA.

G. Pratx and F. Lau are with the Department of Electrical Engineering, Stanford University, Stanford, CA 94305 USA.

C. S. Levin is with the Department of Radiology, Stanford University, Stanford, CA 94305 USA.

II. The System and Timing Method

The RENA-3 ASIC consists of 36 configurable channels of preamplifier, Gaussian Shaper, trigger and timestamp circuitry. Each channel can be configured to accept positive or negative pulses, to act as a trigger or be read out on another channel's trigger. The RENA-3 uses a leading edge discriminator as a trigger. On a trigger, the RENA-3 system records a coarse digital timestamp, two signals for an analog timestamp, and amplitude data from specified channels. One of the basic goals of this work is to calibrate out the time walk inherent to the leading edge discrimination method.

A. *Leading Edge Discriminator Trigger*

The RENA-3 uses a leading edge discriminator to determine event arrival. This consists of a comparator with a programmable threshold value. For a negative pulse, when the input signal passes below the threshold, the RENA-3 records the arrival time. Changing the threshold on one channel while holding another constant shows the pulse shape of the input signal. Fig. 1 demonstrates this effect with a pulser, showing the time difference of two pulses plotted against the changing threshold represented by the comparator voltage.

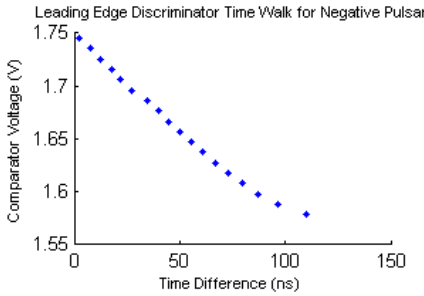

Fig. 1. Changing the threshold value on the leading edge discriminator trigger shows the shape of a pulser. Lowering the threshold causes the negative pulse to fire the comparator at a later time.

B. *Quadrature Timing*

The time difference, used to determine if two events are in coincidence, is found by first examining the coarse digital timestamp and then, if the timestamps are identical or within one count, a fine, analog timestamp [5]. U and V, the quadrature signals of the fast timestamp, are identical

sinusoids with one lagging the other by 90 degrees in phase. In Fig. 2, a plot of U and V signals recorded for several events shows the resulting timing circle. The time difference between two events is calculated by the angular difference between events on the circle, divided by the frequency of the circle, in this case 1 MHz.

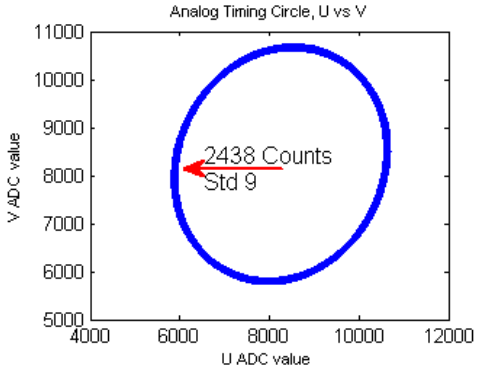

Fig. 2. The quadrature timing signals, U and V, when plotted against each other for many events, form a circle. The fast timestamp is determined by the angular separation of the two events on the circle.

III. Timing Issues

A. ASIC Channel Delay

The most significant effect on timing is from the difference in RENA-3 ASIC channels. There are significant differences in timing delay between channels. This delay could come from a variety of sources, such as variation in path length, differences in comparator delays, or path length difference for the two quadrature signals. Fig. 3 shows a histogram of the time difference from one channel to ten other channels using a pulser input signal. Several distinct Gaussian peaks are present, demonstrating significant variation in the timing delay. A constant offset in timing per channel will appropriately remove the inter-channel delay effect. The improvement in timing dispersion from each calibration for this system are shown later in this paper.

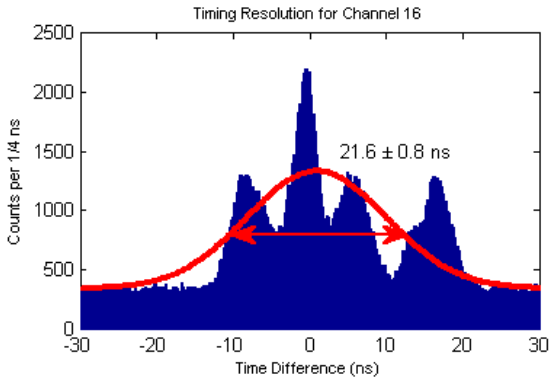

Fig. 3. The pulser timing histogram is shown from one channel to 10 other channels. Randoms are added to the data set and are visible as the constant background level in the histogram. The individual channel delays are visible as the several peaks in the figure.

B. Correlated Quadrature Noise

A second timing effect is also visible from using a pulser. Using pulser data on two channels, plotting the U and V signals against the timing difference shows a non-constant, non-linear correlation between the quadrature signals and time difference. The visible correlation is shown in Fig. 4. This correlation could be the result of the U and V signal coupling in with other circuitry, either on the chip or on the PCB board. Ideally, this would be removed through appropriate shielding. For calibration purposes, a second order fit is adequate to remove the correlated quadrature noise effect.

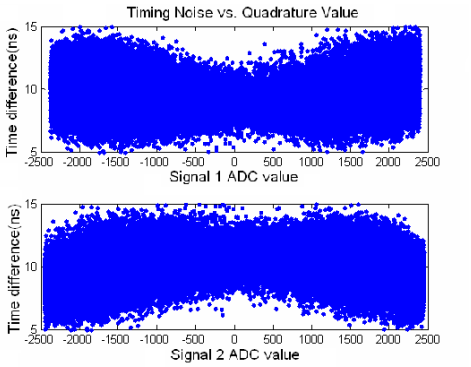

Fig. 4. Plotting the quadrature timing signals against the calculated time difference shows a strong correlation which can be corrected to improve the timing resolution.

C. Crystal-location Dependent Variations on the PSAPD

The PSAPD produces further time dispersion effects. The first is due to the variation in RC time constant across the device. The PSAPD uses a resistive sheet, so charge created by light that enters near the edge or a corner of the device will see an effective resistance significantly lower than that of charge created in the center of the device. The result is an annihilation photon detected by a crystal at the edge of the device will appear to arrive much sooner than those interacting in a crystal near the center. This effect is mentioned in [6], though calibration is not used to correct it. For this system, the time delays for the 8x8 crystal arrays on PSAPDs vary up to 20 nanoseconds [7]. Fig. 5 shows a color map of the time delay for a crystal array after calibration, demonstrating the time delay versus the relative position of the crystals. A constant offset in timing per crystal compensates for this effect.

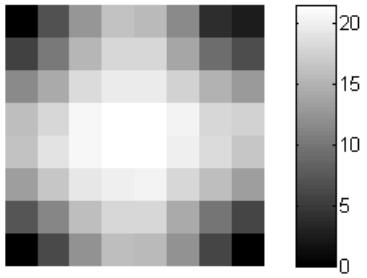

Fig. 5. This color map shows the per crystal timing delay caused by the PSAPD resistive sheet. The color scale units are nanoseconds. The bottom right corner is the reference timing.

D. *Amplitude Dependent Time Walk*

The second effect on timing resolution from the detector is due to energy resolution. The energy resolution of this system is 14.4 ± 0.8% [8]. The different amplitudes of pulses cause the leading edge discriminator to cross its threshold value at different delays. A higher amplitude signal will appear to arrive earlier than a lower amplitude signal. With the imperfect energy resolution of this system, the delay is significant, even when gated for the 511 keV photo peak. A linear adjustment for amplitude will offset a large portion of the delay caused by time walk.

IV. Convex Optimization

A. *Problem Formulation*

The i^{th} event or annihilation photon pair is detected by the system in locations k_1 and k_2. One photon is detected at crystal k_1 and the other photon is detected at crystal k_2. The two arrival times $t_{k1,i}$ and $t_{k2,i}$, are recorded as well as the raw data, column vectors $x_{1,i}$ and $x_{2,i}$. The column vectors contain information such as amplitude and quadrature time samples.

For each crystal, there is a correction function of vector x, $F_k(x)$, which gives an offset, based on the information in x, to correct the reported time, $t_{k,i}$. The time difference for the i^{th} event, Δ_i, between the arrivals of the two photons, as reported by the system, is the difference of the two corrected arrival times as in (1).

$$\Delta_i = (t_{k1,i} - F_{k1}(x_{1,i})) - (t_{k2,i} - F_{k2}(x_{2,i})) \quad (1)$$

To simplify later calibration, the correction function, $F_k(x)$, is chosen to be linear, $a_k' \cdot x$, where a_k is a column vector of coefficients and x is allowed to contain a constant term to correct for bias. Using this correction function the reported time difference is in (2) and rearranged in (3).

$$\Delta_i = (t_{k1,i} - a_{k1}' \cdot x_{1,i}) - (t_{k2,i} - a_{k2}' \cdot x_{2,i}) \quad (2)$$

$$\Delta_i = (t_{k1,i} - t_{k2,i}) - (a_{k1}' \cdot x_{1,i} - a_{k2}' \cdot x_{2,i}) \quad (3)$$

For a small field-of-view PET system, such as our dedicated breast imaging system, time of flight is negligible, and the actual arrival time difference between an event's annihilation photons is negligible. In an unbiased measurement, the expected value of time difference, Δ_i, is zero as in (4).

$$E[\Delta_i] = E[(t_{k1,i} - t_{k2,i}) - (a_{k1}' \cdot x_{1,i} - a_{k2}' \cdot x_{2,i})] = 0 \quad (4)$$

With a small amount of rearranging in (5) and (6), the expected value of the difference in initial arrival times reported is equal to that of the difference in the result of the correction functions.

$$E[t_{k1,i} - t_{k2,i}] = E[a_{k1}' \cdot x_{1,i} - a_{k2}' \cdot x_{2,i}] \quad (5)$$

$$E[t_{k1,i} - t_{k2,i}] = E\left[\begin{bmatrix} x_1' & -x_2' \end{bmatrix}\begin{bmatrix} a_{k1} \\ a_{k2} \end{bmatrix}\right] \quad (6)$$

Equation (6) is the starting point for calibration, and requires finding the coefficients, a_k. Calibration of the system uses known $t_{k1,i}$, $t_{k2,i}$, $x_{1,i}$ and $x_{2,i}$, to determine a_k for all crystals in the system that is consistent with (6) as well as achieves the best timing resolution possible.

B. *Optimization*

In order to achieve the optimum timing resolution, an objective function must be established. A number of methods, such as the L_1 norm or a weighted sum are available to evaluate the timing error. For simplicity, we demonstrate using the L_2 norm, with the system error equaling the sum of the squared time differences for all coincidence events. This formulation is more commonly known as a "least squares problem". In a system with few random coincidences, the L_2 norm will maximize the log-likelihood of the distribution (assuming timing noise is Gaussian distributed). With an initial system calibration scan with a weak source and a low randoms rate, this method works well. However, to adjust the calibration using data from a real scan with a high randoms rate, an alternative cost function, with a smaller penalty for large errors, could be used.

Equation (7) shows an example matrix formulation of the time calibration problem for 5 annihilation photon pairs in a system with 4 crystals. The time differences, $t_{k,i}$, and the raw data column vectors, $x_{1,i}$ and $x_{2,i}$, are known, while the calibration coefficients, a_k, are unknown.

$$\begin{bmatrix} t_{k1,1} - t_{k2,1} \\ t_{k1,2} - t_{k2,2} \\ t_{k1,3} - t_{k2,3} \\ t_{k1,4} - t_{k2,4} \\ t_{k1,5} - t_{k2,5} \end{bmatrix} = \begin{bmatrix} x_{1,1}' & -x_{2,1}' & 0 & 0 \\ 0 & x_{1,2}' & -x_{2,2}' & 0 \\ 0 & 0 & x_{1,3}' & -x_{2,3}' \\ x_{1,4}' & 0 & 0 & -x_{2,4}' \\ 0 & x_{1,5}' & 0 & -x_{2,5}' \end{bmatrix} \cdot \begin{bmatrix} a_1 \\ a_2 \\ a_3 \\ a_4 \end{bmatrix} \quad (7)$$

The vector t (left hand side) is defined to represent all reported time differences. The vector c (right hand side) is the calibration coefficients a_i for each crystal or detector. The matrix A contains the $x_{1,i}$ and $x_{2,i}$ information for all events with each row of the A matrix corresponding to a different coincidence event.

Formulating the convex problem with the L_2 norm amounts to the following least squares problem: select the appropriate vector c to minimize $\| t - A \cdot c \|_2$. This can be directly solved with the pseudo inverse, $c = (A^T \cdot A)^{-1} \cdot A^T \cdot t$. If A becomes large, the inverse of $A^T \cdot A$ can be computationally intensive and other methods such as conjugate gradient or a single-coordinate descent algorithm can be used. The authors in [4] do show a problem formation, but are, in effect, using a single-coordinate descent method, iteratively optimizing for each coordinate, the per crystal delay time.

If the randoms rate is high, we propose using a modified version of the single-coordinate descent method. For each iteration of coordinate optimization, a subset of the data can be optimized. After each iteration, optimizing only across data with near zero time difference allows for less computation as well as removes some of the noise from randoms.

V. Experiments and Results

A. ASIC dependent correction factors from Pulser Data

For the ASIC inter-channel delay calibration, using a single per channel delay, the c vector is a column of the calibration offsets for each channel. One channel is used as a reference and will not have a calibration offset, so the c vector will have one fewer elements than the number of channels. Each row of the A matrix contains one coincidence event. The k^{th} row represents the k^{th} event, recorded between the channel i and channel j. The i^{th} column will contain (+1) and the j^{th} column will contain (-1), representing a corrected time difference for that channel, $t_k - c_i + c_j$; t_k is arrival time difference between channel i and channel j. The size of the A matrix is the number of coincident events rows by the number of channels less the reference channel. Fig. 6 shows the results from a correction for ASIC per channel delay. Additional randoms were added to the data set by arbitrarily pairing list mode data. Before and after application of the algorithm, there is no change to the randoms distribution. The algorithm only improves timing between coincident photons and has no non-linear effects on randoms data. With the delay correction, pulser coincident time resolution is 4.00±0.02 ns.

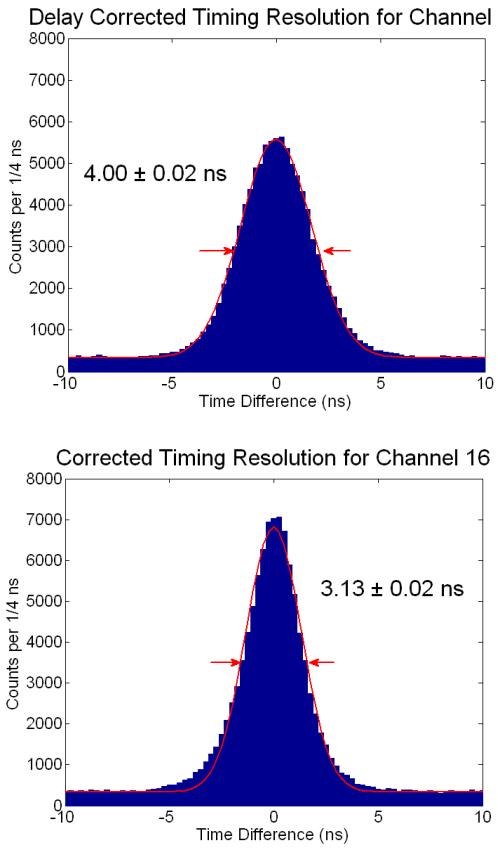

Fig. 6. Timing histograms from one ASIC channel to the other 10 channels using pulser data. Top, the FWHM improved from the uncorrected 21.6±0.8 ns to 4.00±0.02 ns after ASIC inter-channel delay correction. Bottom, correction for quadrature timing correlated noise gains another 22% improvement to achieve 3.13±0.02 ns.

For the pulser data, the quadrature timing variations is an additional known factor that could be calibrated out. This information needs to be added to the A matrix and c vector. A polynomial correction for the two signals, u and v, is achieved by adding coefficients for a correction for each of the channels into the c vector. The number of rows in the A matrix is increased and for each coincident event the recorded signal values are placed into the appropriate column. The right histogram in Fig. 6 includes a quadratic correction to the quadrature signals. The known values, u, v, u^2, v^2, and uv where added into the A matrix, and five additional calibration parameters for each channel where added to c. The constant term is included with constant term from the delay corrections. For 10 channels, there are now 59 calibration parameters. As with the ASIC inter-channel delay correction, the algorithm has no impact on the randoms distribution. With correction for delay and quadrature timing, pulser coincident time resolution becomes 3.13±0.02 ns.

B. Detector-dependent correction of factors

Two 8x8 1x1x1 mm^3 crystal arrays and PSAPDs were connected to one RENA-3 chip. A ^{22}Na point source was placed between the crystal arrays, which were aligned edge-on to the source. The coincidence data were gated to +/-15% around the 511keV photopeak and crystals locations were segmented manually from the acquired crystal image. The setup and floods of the crystal arrays are shown in Fig. 7.

The delay-only convex optimization correction was performed using the direct method of the pseudo inverse. Additional corrections for signal amplitude and quadrature leakage were added. The optimization was performed using a coordinate-descent method, treating the parameters for each crystal location as a different coordinate. For each test, the calibration was performed using a subset of the data; the time resolution is reported using the remaining data.

For this setup, the pre-calibration paired photon coincidence time resolution was found to be 16.37±0.07 ns FWHM (11.58±0.04 ns for unpaired photons). After correction for per crystal location effects, the time resolution improved to 8.42±0.03 ns FWHM. The additional signal amplitude and quadrature timing correction improved coincidence time resolution to 6.92±0.02 ns FWHM (4.89±0.02 ns unpaired photons). Timing histograms are shown in Fig. 8.

The calibration delays resulting from the per crystal PSAPD delay calibration are shown in Fig. 9. The change in RC time constant across the array is visible. The corner crystals have significantly less delay than center crystals and the same pattern is visible in both crystals. There is also an apparent bias between the two crystal arrays. This is due the inherent delay between the PSAPDs readout channels. There is a 20 ns spread in per crystal timing delay caused by the PSAPD RC delay and a 10 ns difference in timing caused by the inherent delay between PSAPDs.

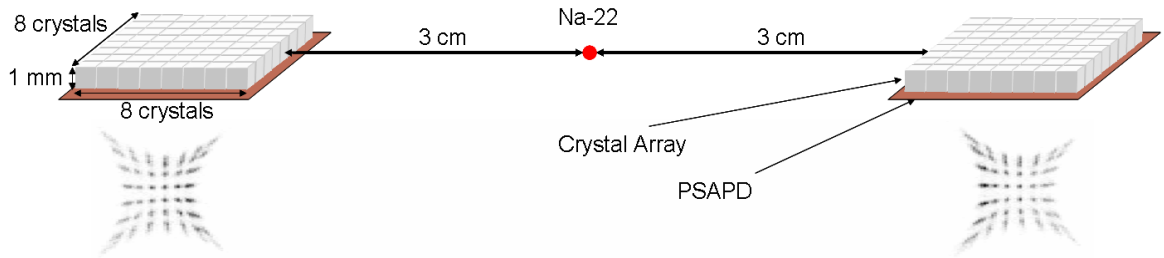

Fig. 7. Two 8x8 1x1x1 mm3 crystal arrays coupled to PSAPDs are placed edge-on, 6 cm apart. A ^{22}Na point source is placed in between the two crystal arrays. The crystal flood histogram for each array used for crystal gating is shown below the crystal.

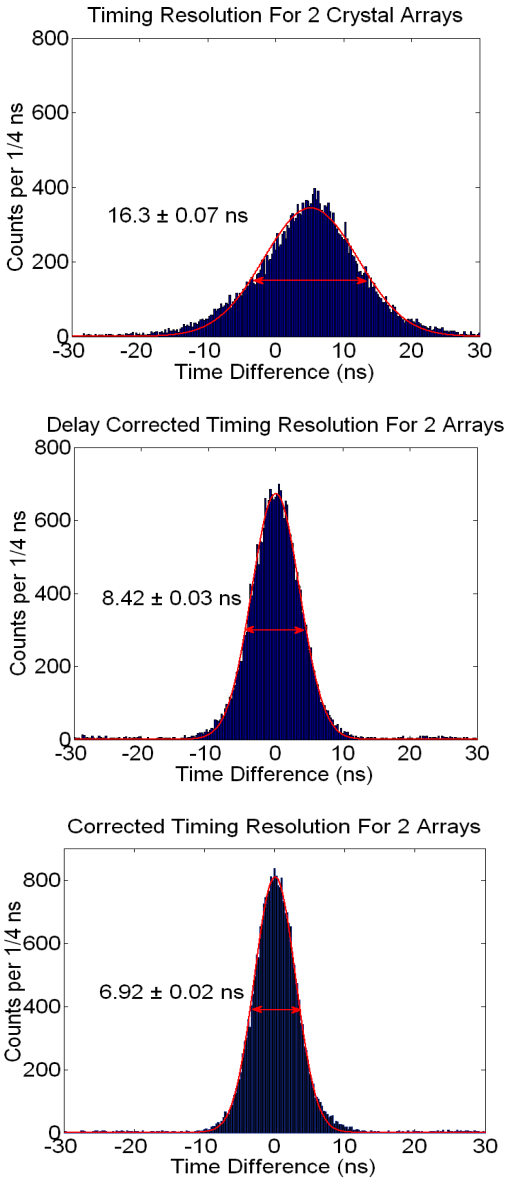

Fig. 8. Timing histograms of coincidence timing between arrays. From top to bottom: No correction, FWHM 16.38±0.05 ns; ASIC inter-channel delay correction, FWHM 8.42±0.03 ns; and inter-channel delay, signal amplitude and quadrature timing correction, FWHM 6.92±0.02 ns.

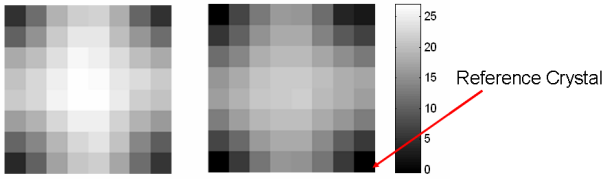

Fig. 9. The optimum delay adjustment for the two 8x8 crystal arrays. The color scale is in nanoseconds.

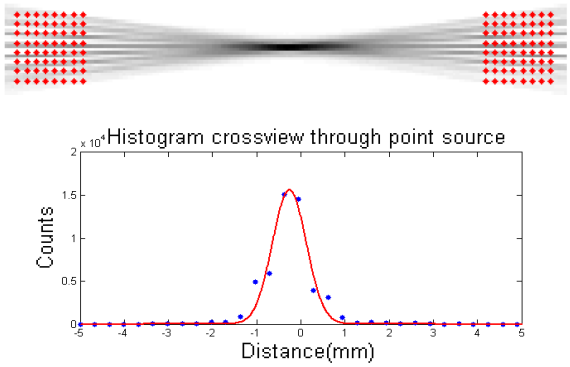

Fig. 10. Histograms of the lines of response from the coincidence data with a 0.250 mm diameter point source with a 0.33 mm pixel/bin size. The bottom plot is a histogram of the lines of response taken from a vertical profile through the center of the point source. The raw FWHM is 0.90 ± 0.05 mm (before beam size deconvolution).

Fig. 10 shows a histogram of the lines of response from the coincidence data. The lines converge at a point source in the middle, confirming that most of the coincidence data were trues. The full width half max of the histogram taken through the point source is 0.90 ± 0.05 mm.

VI. Conclusions

A number of issues can affect timing when using PSAPDs with the RENA-3 ASIC. However, many of these issues are strongly correlated with sources of timing dispersion and can be calibrated out of the system. The system calibration method used was formulated as a convex optimization problem, and by finding the solution, we are able to convert an ASIC with raw timing variation of tens of nanoseconds into a fast timing data acquisition system appropriate for PET. Correcting data for ASIC time channel delay, PSAPD RC time constant delay, leading edge discriminator time walk, and quadrature timing correlated noise, a paired coincidence timing of less than 7 nanoseconds is achieved.

REFERENCES

[1] M.W. Lenox, T. Gremillion, S. Miller, and J.W. Young, "Coincidence Time Alignment for Planar Pixellated Positron Emission Tomography Detector Arrays," in *2001 IEEE Nuclear Science Symposium Conference Record*, San Diego, CA, USA, Nov. 4-10, 2001.

[2] J. J. Williams, "Automated Coincidence Timing Calibration for a Pet Scanner", United States Patent No. 5272344, Dec. 21, 1993.

[3] C.J. Thompson, M. Camborde, M.E. Casey, "A Central Positron Source to Perform the Timing Alignment of Detectors in a PET Scanner," *IEEE Transactions on Nuclear Science*, vol. 52, no. 5, pp.1300- 1304, Oct. 2005.

[4] D. Luo, J. J. Williams, M. K. Limkeman, M. J. Cook, E. L. Oswalt, M. P. Feilen, and D. L. McDaniel, "Crystal-Based Coincidence Timing Calibration for PET Scanner," in *2002 IEEE Nuclear Science Symposium Conference Record*, Norfolk, VA, USA, Nov. 10-16, 2002.

[5] T.O. Tumer, V.B. Cajipe, M. Clajus, S. Hayakawa, A. Volkovskii, "Multi-Channel Front-End Readout IC for Position Sensitive Solid-State Detectors," in 2006 *IEEE Nuclear Science Symposium Conference Record*, San Diego, CA, USA, Oct. 29-Nov. 4, 2006.

[6] Y. Yang, Y. Wu, J. Qi, S. St. James, H. Du, P. A. Dokhale, K.S. Shah, R. Farrell, and S. R. Cherry, "A Prototype PET Scanner with DOI-Encoding Detectors," *The Journal of Nuclear Medicine*, vol. 49, no. 7, pp. 1132-1140, Jul. 2008.

[7] A. Vandenbroucke, A.M.K. Foudray, F.W.Y. Lau, P.D. Olcott, P.D. Reynolds, C.S. Levin, "Performance Characterization of a New High Resolution PET Scintillation detector," in *IEEE Nuclear Science Symposium Conference Record*, 2008.

[8] F.W.Y Lau, A. Vandenbroucke, P.D. Reynolds, M.A. Horowitz, C.S. Levin, "Front-end Electronics for a 1mm^3 Resolution LSO-PSAPD-based PET System with Analog Signal Multiplexing," in *IEEE Nuclear Science Symposium Conference Record*, 2008.